Geomechanics and Engineering, *Vol. 28, No. 5 (2022) 463-475*
https://doi.org/10.12989/gae.2022.28.5.463

Post-pillars design for safe exploitation at Trepça hard rock mine (Kosovo) based on numerical modeling

Gzim Ibishi*[1], Melih Geniş[2a] and Mahmut Yavuz[3b]

[1]*Department of Mining Engineering, Faculty of Geosciences, Mitrovica Isa Boletini University, 40000, Mitrovica, Kosovo*
[2]*Department of Mining Engineering, Faculty of Engineering, Zonguldak Bülent Ecevit University, 67100, Zonguldak, Turkey*
[3]*Department of Mining Engineering, Faculty of Architecture and Engineering, Eskişehir Osmangazi University, 26040, Eskişehir, Turkey*

(Received September 18, 2021, Revised January 20, 2022, Accepted January 24, 2021)

Abstract. In the mine exploitation stage; one of the critical issues is the stability assessment of post-pillars. The instability of post-pillars leads to serious safety hazards in mining operations. The focus of this study is to assess the stability of post-pillars in the 130# stope in the central ore body at Trepça hard rock mine by employing both conventional (i.e., critical span curve) and numerical methods (i.e., FLAC3D). Moreover, a new numerical based index (i.e., Pillar Yield Ratio-PYR) was proposed. The aim of PYR index is to determine a border line between stable, potentially unstable, and failure state of post-pillars at a specific mine site. The critical value of pillar width to height ratio is 2.5 for deep production stopes (e.g., > 800 m). Results showed that pillar size, mining height and mining depth significantly have affected the post-pillar stability. The reliability of numerical based index (i.e., PYR) is verified based on empirical underground pillar stability graph developed by Lunder, 1994. The proposed pillar yield ratio index and pillar stability graph can be used as a design tool in new mining areas at Trepça hard rock mine and for other situations with similar geotechnical conditions.

Keywords: FLAC3D software; hard rock mine post-pillar design; underground excavation

1. Introduction

In underground mining, pillars are defined as the in situ ore or rock left between two or more underground openings (Martin and Maybee 2000, Gao 2018). Pillars are essential support elements of many mining systems. In the majority of underground mines, the role of pillars is to protect underground structures acting as safety barriers in order to provide stable working environment for personnel and mining equipment (Wagner 2003). Ü nlü (2000) noted that stability assessment of pillars is a crucial precondition for safe and economic working condition in underground hard rock and soft mines. Accordingly, accurate pillar stability and design has always been of interest of mining community (Ozbay *et al.* 1995, Kaiser *et al.* 2010, Idris *et al.* 2015). In underground mining, traditionally, stability assessment of pillars is performed calculating the factor of safety according to estimated strength and assumed stress. Thus, for underground safe and good design an accurate estimation of strength and stress is strongly required (Zhang *et al.* 2017).

Pillar strength can be estimated by empirical equations derived by back analyses, whereas, pillar load using tributary area theory and numerical modeling methods. However, a factor of safety is not so indicative for engineering excavations and design. It is not unusual in practice that some underground structures fail and collapse with a factor of safety greater than 1 or remain stable with a factor of safety less than 1; this is also attributed to unknown uncertainties (Wang *et al.* 2002, Van der Merwe and Mathey 2013, Sainoki and Mitri 2017). Over the past years, many studies have been carried out to assess the coal pillars stability using different approaches in order to minimize mining subsidence. For this purpose, coal pillar size has been estimated using of well known empirical methods developed by Salamon and Munro (1967), Mark and Bieniawski (1986), probabilistic design chart approach conducted by Sharipov and Adoko (2021) and numerical modeling methods using appropriate failure criteria (Pariseau *et al.* 1984, Esterhuizen *et al.* 2010, Sherizadeh and Kulatilake 2016, Jessu *et al.* 2018, Jawed and Sinha 2018). However, design of hard rock pillars has not received the same research attention as coal pillars because of irregular mining geometries. Several empirical equations have been developed by different scholars to assess hard rock pillar strength (Hedley and Grant 1972, Von Kimmelmann 1984, Krauland and Soder 1987, Potvin et al. 1989, Sjöberg 1993, Lunder and Pakalnis 1997) and numerical modeling methods using appropriate failure

*Corresponding author, Assistant Professor
E-mail: gzim.ibishi@umib.net
[a]Professor
E-mail: genis@beun.edu.tr
[b]Professor
E-mail: myavuz@ogu.edu.tr

ISSN: 2005-307X (Print), 2092-6219 (Online)

criteria (Martin and Maybee 2000, Mortazavi *et al*. 2009, Kaiser *et al*. 2010, Thibodeau and Yao 2015, Kumar *et al.* 2017, Hemant *et al*. 2017, Ren *et al*. 2020). However, this study provides with a comprehensive brief literature overview on hard rock pillar stability assessment and design criteria used. Martin and Maybee (2000) presented a stability criterion for establishing pillar geometries in hard rock mines based on numerical analyses. Authors carried out a series of numerical analyses applying the finite element program (i.e., Phase2). In order to evaluate the stability of hard rock pillars over the range of width/height ratios from 0.5 to 3, the Hoek-Brown brittle parameters were used and showed a good agreement between the factor of safety lines with the observed previously developed empirical equations (e.g., Lunder and Pakalnis 1997, Hedley and Grant 1972). They noted that a pillar is considered to have failed when the centre of the pillar has a safety factor 1. In this study, the pillar failure involves with the terms as spalling, slabbing and fracturing. The proposed criterion is presented in graphical form with two curves FOS = 1 and FOS = 1.4. Ghasemi *et al.* (2017) developed two models for stability assessment for hard rock pillars based on support vector classification (SVC) and J48 algorithms. Models are supported by pillar stability graph constructed by Lunder and Pakalnis (1997). Authors noted that suggested models have better prediction capacity and their application is easier due to clear graphical outcome. Sjöberg (1993) presented a new methodology for stope roof and sill pillar design for the Zinkgruvan Mine in Sweden. The proposed methodology neither consist empirical formula nor model which can be applied entirely but serve just as a design criterion for rock mechanics engineer for other situations with similar geomechanical conditions. The author suggested to extensive monitoring program in mining areas subjected to high stresses where stope roofs and sill pillars will be loaded at maximum capacity. Lunder and Pakalnis (1997) provided a database of rib pillars histories from different hard rock mines. Authors proposed the confinement formula for determining the pillar strength hard rock pillars. This empirical equation was used to generate pillar stability charts. Also, they plotted the safety factor curves. These curves help plotting all the unstable and failed pillars on the correct side of the line. It is noted that as the confinement in pillar increase so does the pillar strength. Mortazavi *et al*. (2009) presented a study on investigation of the non-linear behavior of rock pillars under natural loading conditions. Authors have validated the numerical results against field data conducted in Canadian hard rock mines by Lunder and Pakalnis (1997).

They noted that there is a fairly good match between numerical and empirical stability pillar graph method. Ren *et al*. (2020) proposed a new mathematical formula predicting the pillar stability. Authors noted that pillar area, rock column area and mining depth play a significant role on pillar stability. Derived calculations from mathematical formula are verified by numerical simulation applying MIDAS-GTS/NX finite element software. The suggested formula can be used for the stability analysis of goafs in similar mines. Schubert and Villaescusa (2008) described a methodology on square and rib mine pillars design at the McArthur River Mine. Authors indicated that the pillar stability graph suggested by Lunder (1994) might be slightly conservative and further adaptation to the site rock mass conditions are required. Oke and Kalenchuk (2017) presented a study selecting the most suitable hard rock pillar design method. It was noted that when there are no available empirical observations, numerical analyses may provide a detailed understanding of pillar behavior. Mitri (2007) provided three methods (i.e., potential stress failure-PSF; energy release rate-ERR; burst potential index-BPI) to assess the stability of crown pillars in deep hard rock mines.

The author noted that the BPI approach is the most suitable among the presented methods, and assess the potential of pillar burst. This method works on the basis of the amount of strain energy stored in the rock as a result of mining activities. In contrast to conventional stress approach which rely on stress only, the author noted that BPI serves as prime indicator of rock failure based on the combined effect of stress and strain, too. The objective of this study was to assess the effects of pillars thickness, mining sequences and mining depth using a finite element, linear elastic analysis software e-z tools developed by the author in 2004. Numerical results are presented in a graphical fashion. Li *et al*. (2013) provided a general methodology with a specific study on minimum required thickness estimation of the crow pillar in a subsea metal mine based on three-dimensional numerical modeling (e.g., FLAC3D). A realistic geometric numerical model was built in SURPAC then exported to FLAC3D by a MATLAB program. Authors noted that such design methodology is helpful to estimate the minimum thickness of crown pillars. Hemant *et al*. (2017) suggested a methodology on crown pillars design for safe mining operation at varying depths.

Authors have developed a statistical model and presented a simple design chart which can be utilized to determine a crown pillar thickness with respect to mining depth in a underground hard rock mine. For this purpose, they conducted 108 nonlinear numerical models with varying rock mass parameters applying ANSYS. From the detailed literature review, it can be clearly seen that each scholar have authentically provided solutions to soft and hard rock pillar stability problems in various underground mines using analytical, empirical and numerical methods.

Compared to other initial studies, the main purpose of this research is to develop a new numerical pillar stability assessment index (i.e., Pillar Yield Ratio) for safe exploitation in an underground hard rock mine. Although a numerous of analytical, empirical and numerical methods have been successfully applied so far, but such numerical index is limited based on literature review. The proposed PYR index together with a pillar stability graph is easy to use for results discussion. Post-pillars compared to other mining pillars (e.g., sill pillar, crown pillar, barrier pillar) left in underground mining systems differ since they have large vertical dimension applied to inclined ore bodies with dip between 30° and 60°. In underground mining, the role of post-pillars is to provide support to hanging wall and back of the stope for a certain period of time during the exploitation stage.

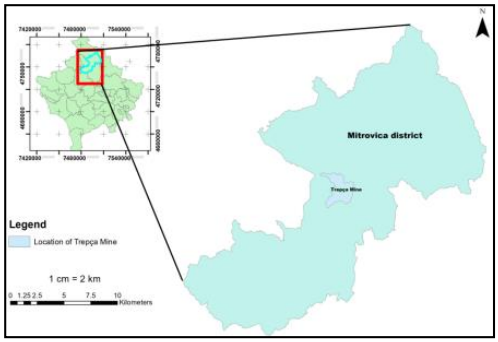

Fig. 1 Mine location map

2. Materials and methods

2.1 Site Investigation

2.1.1 Geological settings

Trepça underground hard rock mine is a poly-metallic mine, located near the Stan Trg village in the Trepça valley, roughly 9 km north-east of Mitrovica district, Kosovo, as given in Fig. 1. Currently, the ore reserves of the mine are supposed to be roughly 20.7 Mt of ore with 4.02% Pb, 4.02% Zn, and 76 g/t Ag (Hetemi 2013). Trepça mineral deposit is located in the Kopaonik block of the western Vardar zone in the further east part of the Dinarides. The Vardar zone comprises of large cost-effective significant mineral deposits of Pb-Zn-Ag-Bi-Mo and small mineral deposit of Cu-Fe-Au (Palinkas *et al*. 2013). Trepça mineral deposit consists of south ore bodies, north ore bodies, and central ore body.

The central ore body is originated by the metasomatic replacement of limestone and consists mainly of an intimate mixture of sulfides associated with little admixed gangue. A geological cross section is given in Fig. 2 showing the central ore body, and the surrounding geological rock units in the study area. The leading sulfides are galena, marmatite, pyrite, and pyrrhotite. As supporting elements of sulfide mineralization appears to be dolomite, calcite, quartz, and rhodochrosite. Geological formation consists of a compressed and folded complex of schist and phyllites, quartzites, and crystalline limestone. In the area close to the mine site, the schist-limestone series, after extreme folding, forms a basement by tuffs and sediments of Miocene age. The marmorized limestone formation in its distorted and folded form localizes the deposition of replacement ore bodies and main fracturing is premineralization and is attributed to early Tertiary movements of Alpine type. Compression stress in the area has been directed chiefly from the northeast developing schistosity and cleavage in the shales and quartzites, and contributing to the obliteration of bedding in the limestone. The regional strike of the competent beds is NW-SE. The breccias-limestone contact forms the directive path for ore solutions, giving rise to replacement deposits in the immediately adjacent limestone. For ore deposition the most favourable conditions are provided by the angle at the junction of the breccias-limestone contact with the schist-limestone contact. The general angle of the central ore body is at an average of about 45°to the north-west that is together with the dip of overlaying schist (Forgan 1950).

2.1.2 Mining method

In the Trepça mine, the overhand cut-and-fill mining method with post-pillar was employed in the central ore body (e.g., 130# stope). The ore body is developed by incline-ramp, and raise in footwall from which several x/cuts are constructed to reach production levels for extraction of mineral resource. The stopes dimensions are approximately 60 m in height, 48 m in width and 72 m in length in the strike direction, with different dimensions of post-pillars (e.g. 6 × 6 m, 8 × 8 m, 10 × 10 m, 12 × 12 m). A typical mining method is shown in Fig. 3.

2.2 Rock mass classification

In this study, typical rock mass classification systems such as Rock Mass Rating – RMR Bieniawski (1989), the Rock Quality Index – Q Barton *et al.* (1974), Grimstad and Barton (1993) and the Geological Strength Index – GSI Marinos and Hoek (2000), were employed to assess the rock mass quality, estimate rock strength parameters and provide preliminary support design for the 130# stope at the +135 m production level based on the stability graph method. Rock mass description and discontinuity measurements were determined in accordance with the suggested methods by ISRM 1981. The RMR system is a widely used empirical design tool in mining and civil projects for rock mass characterization. For rock mass classification purpose, the uniaxial compressive strength of intact rock, rock quality designation, joint condition, joint spacing, joint orientation and ground water are required to be specified. Rock masses of the 130# stope were classified based on the version of RMR_{89}. The Q system was developed at the Norwegian Geotechnical Institute based on more than 200 case histories of underground caverns and tunnels. This system is defined by six parameters including: rock quality designation, number of joint sets, joint roughness, joint alteration, joint water and stress reduction factor. The GSI index was initially developed with the intention to be as practical and simple in application of rock mass characterization as compared to the RMR and Q systems, when used in the Hoek-Brown failure criterion. GSI index is based mainly on the rock mass structure and condition of discontinuities surfaces and is evaluated form visual observations of the rock mass appearance in surface excavations, out-crops and tunnel faces (Bednarek and Majcherczyk 2020). Field investigation results for RMR, Q, and GSI systems are tabulated in Table 1.

2.3 Geotechnical properties of the intact rock and rock mass

2.3.1 Laboratory studies

The lithology of the 130# stope is volcanic breccia (i.e., hanging wall), limestone (i.e., footwall) and the sulfide mineralization (i.e., ore body).

Excavated stopes are backfilled with hydraulic filling materials. The laboratory test result on physical and mechanical properties of the intact rock samples, including unit weight, uniaxial compressive strength, tensile strength, deformation modulus, Poisson's ratio, cohesion and internal

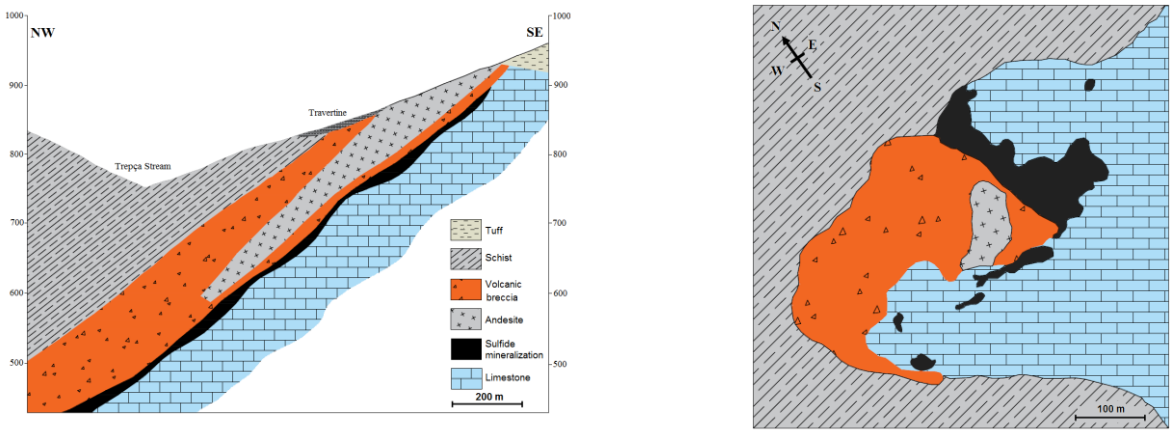

(a) A geological cross-section view (b) A geological plan view

Fig. 2 Mining geology of Trepça hard rock mine (after Forgan 1950)

Table 1 The overall rating estimation for RMR, Q and GSI systems (Ibishi 2019)

Rock type	RMR		Q		GSI	
	Rating range	Mean values	Rating range	Mean value	Rating range	Mean value
Volcanic breccias	54.6-60.1	57.4	0.08-0.85	0.5	55-65	60
Sulfide mineralization	65.8-78.5	72.2	0.3-3.3	1.8	70-80	75
Limestone	60.7-70	65.4	0.1-1.4	0.8	65-75	70

* Rock Mass Rating (RMR); Quality Index (Q); Geological Strength Index (GSI)

Table 2 Physical and mechanical properties of intact rock and backfill material (modified from Hetemi 2013)

Rock type	Unit weight γ (kN/m^3)	Young's modulus E (GPa)	Uniaxial compressive strength σ_{ci} (MPa)	Tensile strength σ_t (MPa)	Poisson's ratio ν	Internal friction angle ϕ (°)	Cohesion c (MPa)
Volcanic breccias	28.4	49.9	60.9	6.4	0.17	51.6	11
Sulfide mineralization	36.3	63.7	78.0	5.9	0.19	56.4	12.2
Limestone	27.3	40.2	59.5	5.0	0.19	51.3	8.8
Backfill material (Abdellah *et al*. 2012, Emad 2017, Naung *et al*. 2018)	-	1.4	1.6	0.01	-	34.5	1.2

friction angle, are listed in Table 2, whereas, mechanical properties of the hydraulic backfilling materials are adapted from the literature.

2.3.2 Rock mass parameters

Rock mass parameters (e.g., tensile strength, deformation modulus, cohesion and internal friction angle) are the fundamental input parameters required for numerical analysis. Due to high cost and very complex measurement process of the rock mass deformation modulus (E_m), empirical equations are much more convenient tools for design purposes (Zhou *et al.* 2019). The estimation procedure is as follows: every single empirical equation is used to obtain a value of a deformation modulus then extreme values (i.e., minimum and maximum) are omitted and the average value of calculated deformation modulus is accepted as a feasible value for different rock types. The same procedure is applied for determining the tensile strength, cohesion and internal friction angle. In addition, estimation of the bulk (K) and shear (G) modulus are given in Table 3.

2.4 Geotechnical problem observed in Trepça mine

In general, geotechnical instability problems observed in 130# stope at Trepça mine are related to rock falls and/or spalling due to presence of high in situ stress state, large stope geometry, previously poor design of post-pillars and unfavorable geological structures, as given in Fig. 4. An investigation was conducted by Zeqiri (2020) to understand the causes of mining accidents in deep production stopes, as a result of rock falling and/or spalling from the back of the stope and sidewalls an official report concludes that 232 minor injuries, 12 serious injuries and one fatality was occurred in a period of time from 2007 to 2011.

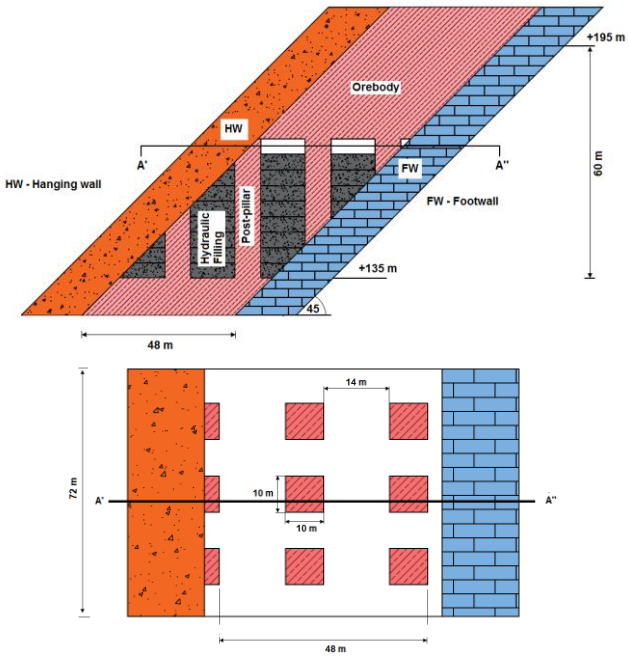

Fig. 3 A typical overhand cut-and-fill mining with post-pillars left in the 130# stope. *Not to scale*

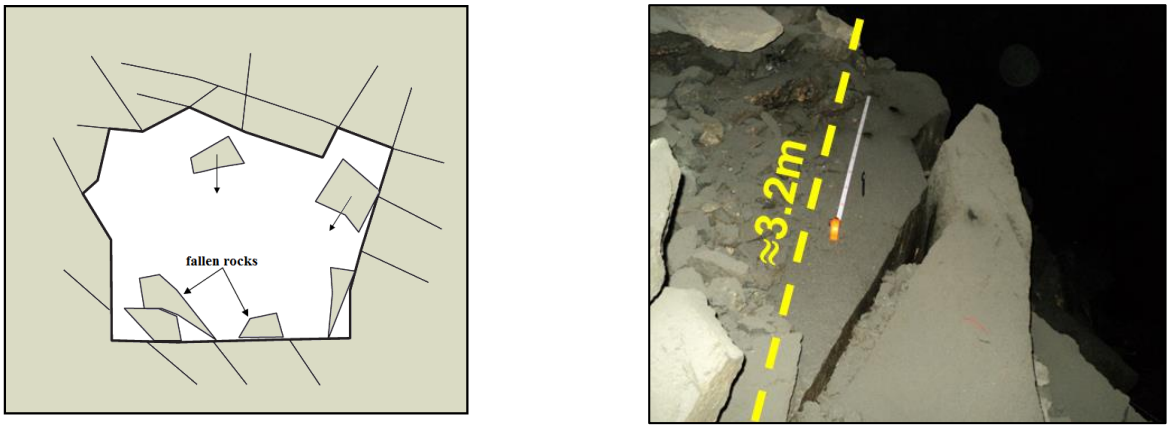

(a) General schematic representation of rock falling (b) Fallen rock from the back of stope at a depth of 693 m between two post-pillar at a distance approximately 20 m

Fig. 4 Stope instability problems observed in the Trepça underground base metal mine

Accordingly, the cause of these failures are triggered from different origins such as the presence of high in situ stress state (i.e., vertical stress increasing with depth tending to be a hydrostatic state in deep environments), large opening geometry, poor design of post-pillars and stopes, and excessive vibration levels induced by blasting practices. The key point in this analysis is that how rock mass surrounding an underground production stope yields and how post-pillars acts to control the amount of yielding zone due to increasing mining height and depth. For this purpose, safe yielding zone estimation (i.e., PYR) was necessary to identify post-pillars whether are stable or unstable. Optimization of post-pillar geometry and size is very important, since, oversized post-pillars cause potential ore losses while undersized post-pillars may cause failure and instability problems in the production stopes (Paveley and Harding 2011).

Thus, Span Design Curve (SDC) is one of the empirical methods most widely used to preliminarily determine the allowable unsupported span of deep underground openings between two post-pillars, mainly based on RMR system (Wang *et al*. 2000). For this purpose, RMR systems was used as convenient tools due to their absence of complication and practical use, and recommended by the geotechnical engineers in the preliminary design phases of underground excavations projects.

2.5 Empirical analysis

2.5.1 Stability analysis based on Critical Span Curve

In rock engineering, obtaining reliable stability analysis and support units is one of the most difficult tasks (Geniş and Çolak 2015). Therefore, the critical span curve empirical method was used to design maximum allowable

Table 3 Geomechanical rock mass properties

Author(s)	Rock mass deformation modulus, E_m (GPa)	Eq.	*OB	FW	HW
Bieniawski (1978)	$E_m = 2 \cdot \mathrm{RMR} - 100$	(1)	44.4	30.8	14.8
Serafim and Pereira (1983)	$E_m = 10^{\left(\frac{\mathrm{RMR}-10}{40}\right)}$	(2)	35.9	24.2	15.3
Nicholson and Bieniawski (1990)	$E_m = \frac{E_i}{100}\left[0.0028 \cdot \mathrm{RMR}^2 + 0.9 \cdot \mathrm{e}^{\left(\frac{\mathrm{RMR}}{22.82}\right)}\right]$	(3)	22.9	11.1	10.1
Aydan *et al.* (1997)	$E_m = 0.0097 \cdot \mathrm{RMR}^{3.54}$	(4)	36.8	25.9	16.3
Read *et al*. (1999)	$E_m = 0.1 \cdot (\mathrm{RMR}/10)^3$	(5)	37.6	27.9	18.9
Aydan *et al.* (2012)	$E_m = \mathrm{RMR}/(\mathrm{RMR} + 6(100 - \mathrm{RMR})) \times E_i$	(6)	19.2	9.6	9.1
Gökçeoğlu *et al*. (2003)	$E_m = 0.0736\mathrm{e}^{0.0755\times\mathrm{RMR}}$	(7)	17.1	10.2	5.6
	$E_m = 0.1451\mathrm{e}^{0.0654\times\mathrm{GSI}}$	(8)	19.6	14.1	7.3
Ramamurthy (2004)	$E_m = E_i \cdot \mathrm{e}^{\left(\frac{\mathrm{RMR}-100}{17.40}\right)}$	(9)	12.9	5.5	4.3
	$E_m = E_i \times \mathrm{e}^{0.8625\times\mathrm{Q}-2.875}$	(10)	16.9	4.5	4.3
Galera *et al*. (2018)	$E_m = 0.0876 \cdot \mathrm{RMR}$	(11)	6.3	5.7	5.0
	$E_m = 0.0876\mathrm{RMR} + 1.056(\mathrm{RMR} - 50) + 0.015(\mathrm{RMR} - 50)^2$	(12)	37.1	25.5	13.6
Khawar (2013)	$E_m = 1.35 \times \mathrm{e}^{0.047\ \mathrm{RMR}}$	(13)	40.2	29.1	20.0
Vasarhelyi and Kovacs (2017)	$E_m = E_i \times \mathrm{e}^{\left(\frac{\mathrm{RMR}-100}{22.94}\right)}$	(14)	18.9	8.9	7.8
Barton (2002)	$E_m = 10 \times \mathrm{Q_c}^{1/3} = 10 \times \left(\mathrm{Q} \times \frac{\sigma_{\mathrm{ci}}}{100}\right)^{1/3}$	(15)	11.1	7.8	6.7
	$E_m = 10^{\left(\frac{15\log\mathrm{Q}+40}{40}\right)}$	(16)	11.0	9.6	8.9
Hoek and Brown (1997)	$E_m = 10^{\left(\frac{\mathrm{GSI}-10}{40}\right)}\sqrt{\frac{\sigma_{\mathrm{ci}}}{100}}$	(17)	37.2	24.3	13.8
Sönmez *et al.* (2004)	$E_m = E_i \times \left(\mathrm{e}^{\left(\frac{\mathrm{GSI}-100}{9}\right)^a}\right)^{0.4}$	(18)	36.5	30.5	20.5
	$E_m = \left(1 - \frac{\mathrm{D}}{2}\right)\sqrt{\frac{\sigma_{\mathrm{ci}}}{100}}\,10^{\left(\frac{\mathrm{GSI}-10}{40}\right)}$	(19)	22.3	14.6	8.3
Hoek and Diederichs (2006)	$E_m = 0.33\mathrm{e}^{0.064\times\mathrm{GSI}}$	(20)	40.1	29.1	15.3
	$E_m = E_i \times \left(0.02 + \frac{1 - \mathrm{D}/2}{1 + \mathrm{e}^{(60+15\ \mathrm{D}-\mathrm{GSI})/11}}\right)$	(21)	22.9	17.4	8.3
	Average values:		26.1	17.4	11.0
Aydan *et al.* (2012)	$\sigma_{tm} = RMR/(RMR + 6(100 - RMR)) \times \sigma_{ti}$	(22)	1.7	1.1	1.1
	$c_m = RMR/(RMR + 6(100 - RMR)) \times c_i$	(23)	3.6	2.1	2.0
	$\phi_{mass} = \left(0.3 + 0.7\frac{RMR}{100}\right) \times \phi_i$	(24)	45.4	38.7	36.2
$K = \frac{E}{3(1-2\nu)}$		(25)	14.1	8.8	5.6
$G = \frac{E}{2(1+\nu)}$		(26)	10.9	7.4	4.7

*OB: Ore body; FW: Footwall; HW: Hanging wall; For GSI ≥ 30, a = 0.5, D=0.8 (poor blasting)

span between post-pillars in 130# stope. This graph was initially developed by Lang (1994) to evaluate roof stability in underground mines which utilize the cut-and-fill mining method on the basis of 172 data sets classified with RMR_{76} classification system for good rock mass ranging from 60 - 80. This graph was initially developed by Lang (1994) to evaluate roof stability in underground mines which utilize the cut-and-fill mining method on the basis of 172 data sets classified with RMR_{76} classification system for good rock mass ranging from 60 - 80. Later on, in 2003 the database was updated with 292 data sets with case histories from an additional six mines, more than 60% of the database consists of good rock, as presented in Fig. 5 (Ouchi *et al.* 2004). Accordingly, Fig. 5 illustrates the span design curve where it can be seen that for an average value of RMR_{89}=72 and span of approximately 20 m, the 130# stope was located in the potentially unstable zone, in fact the span of 20 m between two post-pillars at the Trepça underground base metal mine was unstable adding also the mining height, large in situ stress state environment and uncontrollable design of post-pillar dimensions contributed to this situation.

It is indicative that the bearing capacity of post-pillars decreases with span width increase. Acting in this way has helped us to more easily understand leaving post-pillars at a

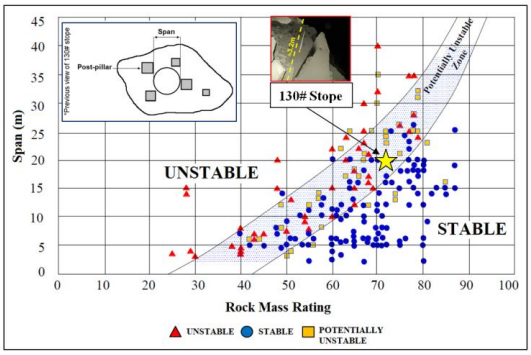

Fig. 5 Preliminary stability assessment of the 130# stope based on the critical span curve empirical method

controlled distance. In 130# stope, the mining height was observed to be out of control, neglecting the safety regulations at work injuries and fatalities are unpredictable.

In this study, to correctly analyze the stability of the post-pillars and the area of influence, we first applied critical span curve empirical method. These empirical methods cannot appropriately provide distribution of displacements, yield zones and stresses. For this purpose, the Itasca's software FLAC3D was utilized to understand post-pillars behavior and assess its stability based on a new Pillar Yield Ratio (PYR) index.

2.6 Pillar stability assessment index

In the following, a new Pillar Yield Ratio (PYR) index is described, which is used as a basis for the numerical model results interpretation.

2.6.1 Pillar Yield Ratio (PYR) index

The extent of failure zones is the most widely criterion used in numerical modeling when the elastic-plastic solution is employed. The rock failure is reached when rock mass is loaded beyond its elastic limits; however, such criterion is used to evaluate post-pillar instability. New assessment index is used as a basis for the interpretation of numerical results applied to the assessment of geotechnical stability of the modeled post-pillars for overhand cut-and-fill stoping method is developed. The Pillar Yield Ratio (PYR) is used to determine a border line between stable, potentially unstable, and failure state of post-pillars. PYR was developed to compare of potential instabilities of post-pillars under different mining conditions (e.g. dimension of pillars, mine excavation height and mining depth). In this assessment index, the percentage of yield domain area of the pillar is calculated according to Eq. (27) to Eq. (29). The post-pillar instability takes place when the extent of failure zones exceeds 35%.

$$(PYR)_{CC} = \frac{A_Y}{w_p \times w_p} = \frac{A_Y}{A_{pCC}} \times 100\% \quad (27)$$

$$(PYR)_{AA} = \frac{A_Y}{w_p \times h_p} = \frac{A_Y}{A_{pAA}} \times 100\% \quad (28)$$

$$(PYR)_{BB} = \frac{A_Y}{w_p \times h_p} = \frac{A_Y}{A_{pBB}} \times 100\% \quad (29)$$

Where;

(PYR) - is the Pillar Yield Ratio,
(AY) - is the total yield domain area of the pillar,
(A_{pCC}) - is the total domain area of the pillar in horizontal cross section (i.e. plan view),
(A_{pAA}) - is the total domain area of the pillar in vertical cross section (i.e. side view),
(A_{pBB}) - is the total domain area of the pillar in vertical cross section (i.e., front view).

Both shear and tension failure modes are considered in calculation procedure using Eqs. (27)-(29). The yield ratio in percentage (%) is obtained based on cumulative number of failed domain area of the pillar (AY) to the total domain area of the pillar (AP). If the yield domain area of the pillar is '100' this indicate total failure state and when the yield domain of the pillar is '0' this indicate none failure state. Further, yielding will be considered as a rule for post-pillar instability performance, as presented in Table 4. A rule of thumb being used in this assessment index is taking into account the highest PYR values of the yield domain area after comparing three different cross section views of post-pillar, as shown in Fig. 6. During numerical analysis results, it has been felt the need to develop a classification index to define the post-pillar failure state more precisely, without judging only the visual extent of the failure zones in a pillar or describing in words as failed or partially failed. Herein, the main objective of PYR assessment index is to determine whether the pillar is stable, potentially unstable, or failed (see Table 4). Furthermore, a new Pillar Stability Graph (PSG) is proposed for the Trepça mine following the principle of PYR classification index. PSG is developed mainly based on Lunder's graph. The PSG is originally a site-specific database for the Trepça mine that investigates the minimum allowable pillar dimensions to be left in stope, see Fig. 7.

Table 4 Pillar Yield Ratio (PYR)

Description	Rating (%)
Stable state	0 ≤ PYR < 35
Potentially unstable state	35 ≤ PYR < 60
Failure state	60 ≤ PYR < 100

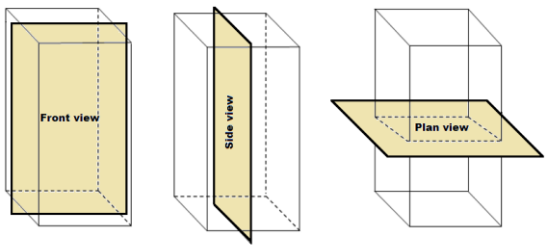

Fig. 6 Post-pillar cross-section view

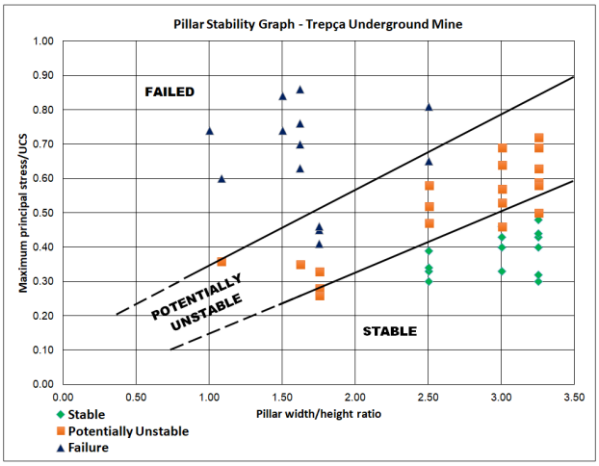

Fig. 7 A typical pillar stability graph

3. Results and discussions

To investigate the stability of the post-pillars in overhand cut-and-fill mining method and verify the empirical results presented in Section 2.5.1, the finite difference modeling software FLAC3D (Fast Lagrange Analysis of Continua) version of 3.0 of Itasca (2005) was utilized. With the help of numerical analysis it is possible to investigate the plastic zones and stress distribution around production stopes and in post-pillars during each mining sequence.

3.1 FLAC3D modeling

A typical geometry problem of the 130# stope given in Fig. 3, with dimensions 60 m in vertical height, 48 m in width, 72 m in length in the strike direction and the stope was inclined at an angle of 45° from horizontal. In order to minimize the effects in the mining sequence, the model was created with dimensions of 148 m wide (x-direction), 216 m long (y-direction) and 140 m high (z-direction) with 371520 zones and 394192 grid points were defined, the generated model is illustrated in Fig. 8. Fig. 8(b), illustrates half of the model in y-direction due to symmetry of the stope geometry and other conditions. Different mesh sizes are used to obtain accurate numerical results. A denser mesh size was adopted around the area of interest (i.e., post-pillar, excavation) to increase accuracy. Model is constructed using brick-shaped mesh. The rock mass assumed to be elastic-perfectly-plastic material. Physical and mechanical properties of the rock mass and backfill properties were determined in Section 2.3. To identify elements subjected to yielding and plastic behavior in the post-pillars and around stopes the Mohr-Coulomb strength criterion was utilized. Numerical models include 8 mining steps. The displacement boundary conditions of the model consist of (1) fixed in x-direction displacement at the right and left boundaries, (2) fixed in y-direction displacement at the back and front of the boundaries, (3) fixed z-direction displacement at the bottom and at the top of the boundary. Vertical (Pv) and horizontal (Ph) stresses were applied on the upper boundary and perpendicular to the strike of the ore body. Vertical stress is a function of the overburden. In this research the ratio of horizontal to vertical stresses is assumed to be (k = 1) as suggested by Hoek (2003). Unfortunately, there is no in situ stress measurement in the mine site. Thus, the estimated vertical in situ stresses are tabulated in Table 5. After defining the constitutive relation, rock mass strength parameters', assigning boundary conditions and initial stress state, then the model was run until the equilibrium stage has been achieved.

Table 5 Hydrostatic in situ stresses for numerical modeling

Depth (m)	$P_V=P_H$
473	12.2
573	15.4
693	18.7
813	21.9
933	25.1

3.2 Numerical results

This study is a contribution to the stability analysis and post-pillar pattern design for deep production stopes and large span at the Trepça hard rock mine using empirical and numerical methods. Numerical models include 8 mining steps. As mining advances upwards, the backfilling sequence fills the initial layer with hydraulic filling after mining the next layer, see Fig. 8(b). These analyses include post-pillars with same dimensions and different mining heights, see Table 6. Numerical analyses show the failure zone distribution in each mining step (Figs. 9 and 10). The extent of failure zones in the 130# stope and post-pillars are presented in Fig. 9, and illustrate extension of failure zone in post-pillars as mining height increases gradually from 4 m to 12 m. The maximum extent of failure zone reaches PYR = 100 % when mining height is 12 m (Fig. 10(c)). In Fig. 10, left pictures indicates the front view of the central ore body (Fig. 8(b)), whereas, the right pictures indicates the plan view. It can be clearly seen that the failure zone extends in post-pillars as mine excavation height increases. Whereas, the lowest value of the failure zone in post-pillars located in the hanging wall side of the stope is 30%, as seen in Fig. 10(a), since the mine excavation height reaches 4 m. The highest value of the failure zone in post-pillars located at the footwall side of the stope is 100%, as seen in Fig. 10(c), since the mine excavation height reaches 12 m.

For post-pillars with dimensions of 12 m × 12 m, the allowable mine excavation height is 4 m. Fig. 10 shows the mine excavation height with respect to the extent of failure zones in post-pillars. Another model, where the optimal mining height is recommended 4 m and mining depth range from 453 m to 933 m below the ground surface is summarized in Table 7.

Numerical simulations have been performed to examine the effect of mining depth on the post-pillars stability based on PYR index. The highest value of the failure zone in post-pillars located at the footwall side of the stope is 55%, as given in Fig. 12(e), since the mine excavation depth reaches 933 m. Whereas, the lowest value of the failure zone in

Table 6 Maximum extent of failure zones in post-pillars at a mining depth of 693 m

Zone	Mining height (m)	Maximum extent of failure zone (%)					
		Hanging wall			Footwall		
		HW1	HW2	HW3	FW1	FW2	FW3
Post-pillar (12×12) m	4	31	30	31	51	59	51
	8	54	53	55	90	91	90
	12	74	79	74	100	100	100

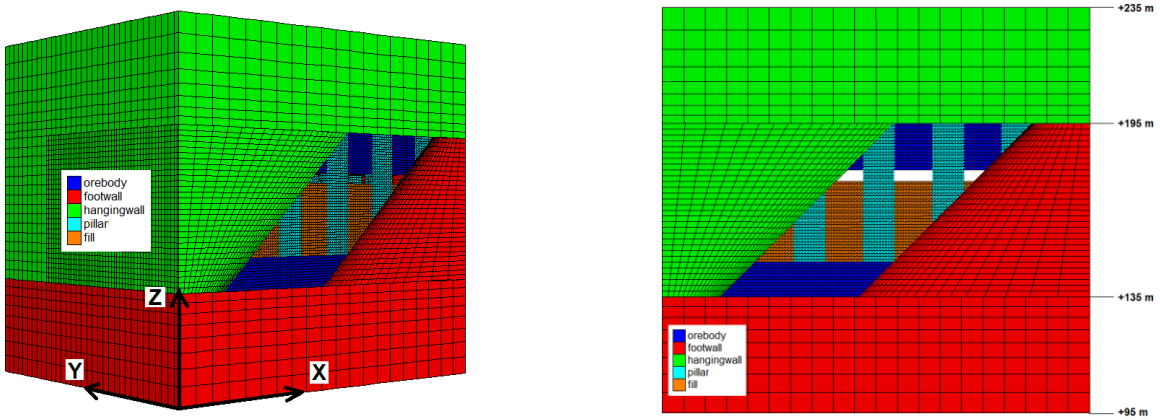

(a) 3D numerical model (b) Vertical section in the x-z plan

Fig. 8 Generated numerical model of the 130# stope

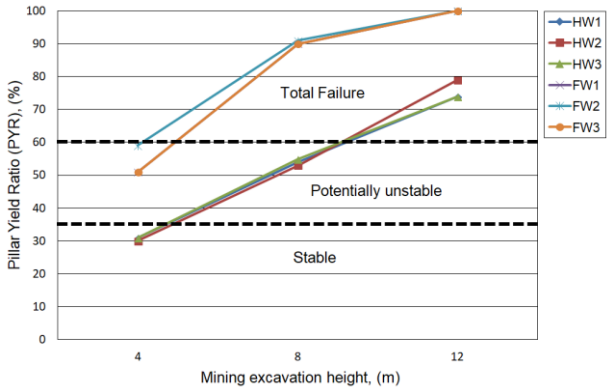

Fig. 9 Mine excavation height vs. extent of failure zones in post-pillars of the 130# stope with the mining and backfilling sequence fill

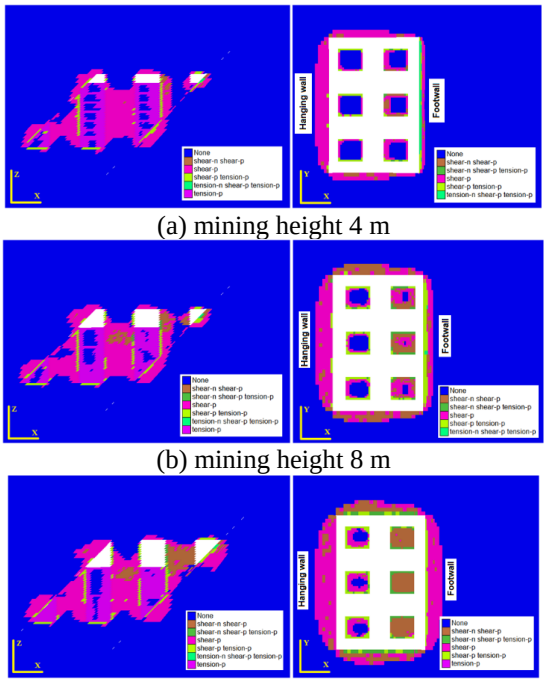

(a) mining height 4 m

(b) mining height 8 m

(c) mining height 12 m

Fig. 10 Maximum extent of failure zones in post-pillars and surrounding stope

post-pillars located at the hanging wall side of the stope is 26%, as seen in Fig. 12(a), since the mine excavation depth reaches 453 m. To understand easily the PYR results, a graph is provided in Fig. 11.

From numerical results it can be concluded that increasing mine excavation height when extraction process is being carried out at a certain depth, post-pillars are indicated to lose bearing capacity, as result span width of 130# stope more than 10 meters increase the probability of stope collapse, see Figs. 4 and 5. The allowable mine excavation height should be kept 4 meters and seems to be much more stable when the ratio of post-pillar width to height ratio is equal or more than 2.5. Post-pillars left on the footwall side seems to be potentially unstable due to the fact that are located almost in the centre of the mined-out stopes and are meant to support the whole back of the stope. Fig. 12 illustrates the extent of failure zones increases gradually with the increase of mine excavation depth. Failure zone has also extended in sidewalls (e.g., hanging wall and/or

Table 7 Maximum extent of failure zones in post-pillars at a mining depth ranging from 453 m to 933 m

Zone	Mining height (m)	Maximum extent of failure zone (%)					
		Hanging wall			Footwall		
		HW1	HW2	HW3	FW1	FW2	FW3
Post-pillar (13×13) m	453	27	27	27	26	31	26
	573	28	28	28	36	39	36
	693	29	28	29	45	47	44
	813	30	31	30	19	55	49
	933	31	30	32	54	55	52

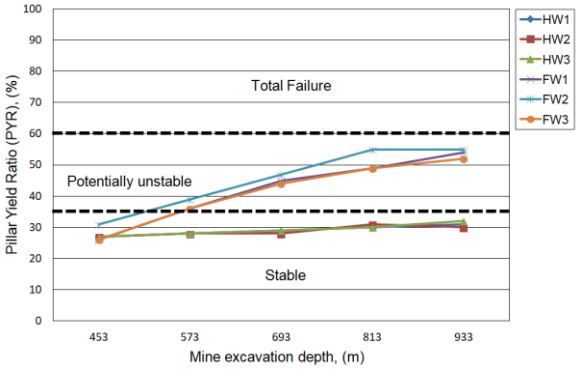

Fig. 11 Mining depth vs. extent of failure zones (PYR) in post-pillars of the 130# stope with the mining and backfilling sequence fill

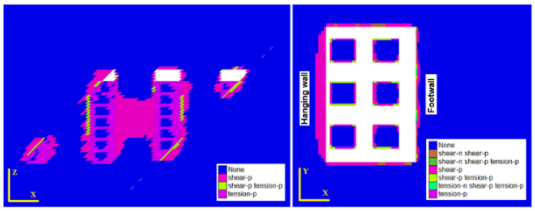

(a) mining depth 453 m

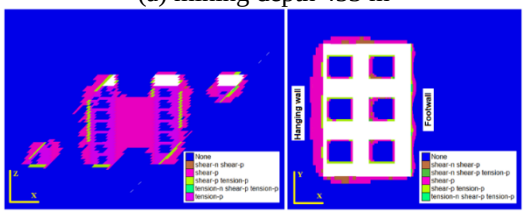

(b) mining depth 573m

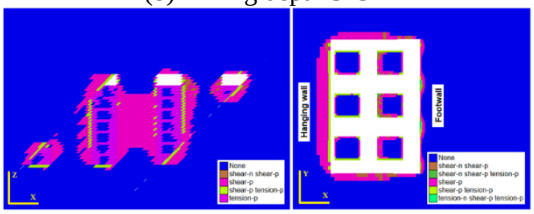

(c) mining depth 693 m

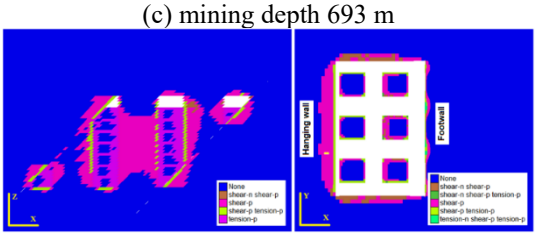

(d) mining depth 813 m

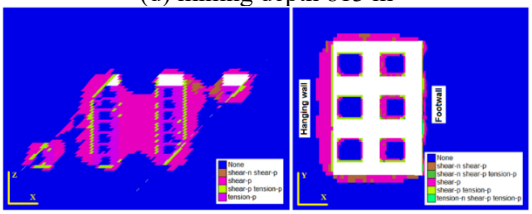

(e) mining depth 933 m

Fig. 12 Extent of failure zones in post-pillars with modeling mine excavation depths

footwall). Post-pillars are designed to gradually yield below the lower levels.

4. Conclusions

In this study, the stability of post-pillars for overhand cut-and-fill stoping method has successfully been investigated employing both the empirical (i.e., Span Design Curve) and numerical methods (i.e., FLAC3D). Conducted numerical analysis investigated the effect of post-pillars width to height ratio and mining depth. This research has attempted to determine the most optimal excavation height and minimum required size of post-pillars under hydrostatic stress conditions. From the numerical analysis results it is carefully observed that exceeding of mine excavation height more than 4m, deep underground production stopes can suffer from serious ground problems where failure zone and maximum principal stresses occur in the hanging wall and footwall as the main ore body has low dip angle 45°. In deep production stopes, mine excavation height is suggested to be as maximum mine excavation height as 4m and post-pillar dimension should be at least (width/height ≥ 2.5). The critical value of pillar width to height ratio is 2.5 for deep production stopes (e.g., > 800 m). When the pillar width to height ratio is greater than 2.5 the pillar condition is stable ($0 \leq PYR \leq 35$). When the pillar width to height ratio is less than 2.0 the pillar condition is potentially unstable ($35 \leq PYR \leq 60$), and when the pillar width to height ratio is below 1.0 ($60 \leq PYR \leq 100$), the pillar completely fail. Stability assessment of post-pillars is accomplished based on new developed assessment index. The Pillar Yield Ratio (PYR) and Pillar Stability Graph (PSG) enable post-pillars to be divided into three main classes as; stable state, potentially unstable state, and failed

state. The proposed assessment index takes into account the extent of failure zones based on elastic-plastic solution. The limitations of this research are lack of in situ stress measurements and back analysis allowing the refinement of the numerical model.

Acknowledgments

The research described in this paper was financially supported by the Scientific Research Project Supporting Commission of Eskişehir Osmangazi University [grant number 201715A238].

References

Abdellah, W., Mitri, H.S., Thibodeau, D. and Moreau-Verlan, L. (2012), "Stochastic evaluations of haulage drift unsatisfactory performance using random Monte-Carlo simulation", *Int. J. Min. Eng*., **4**(1), 63-87. https://doi.org/10.1504/IJMME.2012.048000.

Aydan, Ö., Tokashiki, N. and Geniş, M. (2012), "Some considerations on yield (failure) criteria in rock mechanics", *Proceedings of the 46th US Rock Mechanics Geomechanics Symposium*, Chicago.

Aydan, Ö., Ulusay, R. and Kawamoto, T. (1997), "Assessment of rock mass strength for underground excavations", *Proceedings of the 36th US Rock Mechanics Symposium*, New York.

Barton, N. (2002), "Some new Q-value correlations to assist in site characterisation and tunnel design", *Int. J. Roc. Mech. Min. Sci*., **39**(2), 185-216. https://doi.org/10.1016/S1365-1609(02)00011-4.

Barton, N., Lien, R. and Lunde, J. (1974), "Engineering classification of rock masses for the design of tunnel support", *Roc. Mech*., **6**(4), 189-236.

Bednarek, L. and Majcherczyk, T. (2020), "An analysis of rock mass characteristics which influence the choice of support", *Geomech. Eng*., **21**(4), 371-377. https://doi.org/10.12989/gae.2020.21.4.371.

Bieniawski, Z.T. (1978), "Determining rock mass deformability: experience from case histories", *Int. J. Roc. Mech. Min. Sci. Geomech*., **15**, 237-247.

Bieniawski, Z.T. (1989), "Engineering Rock Mass Classification", Wiley, New York.

Emad, M.Z. (2017), "Numerical modelling approach for mine backfill", *India Academy of Science*, **42**(9), 1595-1604. https://doi.org/10.1007/s12046-017-0702-0.

Esterhuizen, E., Mark, C. and Murphy, M. (2010), "Numerical model calibration for simulation coal pillars, gob and overburden response", *Proceeding of the 29th international conference on ground control in mining*, Margantown.

Forgan, C.B. (1950), "Ore deposits at the Stan Trg lead-zinc mine", *Proceedings of the 18th International Geological Congress*, London.

Galera, J.M., Alvarez, M. and Bieniawski, Z.T. (2005), "Evaluation of the deformation modulus of rock masses: comparison of pressuremeter and dilatometer tests with RMR prediction", *Proceedings of the ISP5-PRESSIO International symposium*, Madrid.

Gao, W. (2018), "Influence of interaction between coal and rock on the stability of strip coal pillar", *Geomech. Eng*., 14(5), 499-507. https://dx.doi.org/10.12989/gae.2018.14.5.499

Geniş, M. and Çolak, B. (2015), "Stability Assessment of the Gökgöl Karstic Cave (Zonguldak, Turkey) by Analytical and Numerical Methods", *Roc. Mech. Roc. Eng*., **48**(6), 2383–2403. https://doi.org/10.1007/s00603-014-0700-z.

Ghasemi, E., Kalhori, H. and Bagherpour, R. (2017), "Stability assessment of hard rock pillars using two intelligent classification techniques: a comperative study", *Tunn. Undergr. Sp. Technol*., **68**, 32-37. https://doi.org/10.1016/j.tust.2017.05.012.

Gökçeoğlu, C., Sönmez, H. and Kayabaşi, A. (2003), "Predicting the deformation moduli of rock masses", *Int. J. Roc. Mech. Min. Sci*., **40**, 701-710. https://doi.org/10.1016/S1365-1609(03)00062-5.

Grimstad, E. and Barton, N. (1993), "Updating of the Q-system for NMT", *Proceeding of the international symposium on sprayed concrete-modern use of wet mix sprayed concrete for underground support. Norwegian Concrete Association*, Oslo, Norway.

Hedly, D.G.F. and Grant, F. (1972), "Stope-and-pillar design for the Elliot lake uranium mines", *Bull. Can. Inst. Min. Metall*., **65**, 37-44.

Hemant, K., Debasis, D. and Chakravary, D. (2017), "Design of crown pillar thickness using finite element method and multivariate regression analysis", *Int. J. Min. Sci. Technol*., **27**, 955-964. https://doi.org/10.1016/j.ijmst.2017.06.017.

Hetemi, M. (2013), "Contribution to the optimal modeling of mine field opening from level XI to level XIII in Stan Trg mine", Ph.D. Dissertation. University of Prishtina, Prishtin Dissertation. University of Prishtina, Prishtina.

Hoek, E. and Brown, E.T. (1997), "Practical estimates or rock mass strength", *Int. J. Roc. Mech. Min. Sci. Gem. Abst*., **34**(8), 1165-1186.

Hoek, E. and Diederichs, M.S. (2006), "Empirical estimation of rock mass modulus", *Int. J. Roc. Mech. Min. Sci*., **43**(2), 203-215. https://doi.org/10.1016/j.ijrmms.2005.06.005.

Ibishi, G. (2019), "Stability Assessment of Post Pillars in Cut-and-Fill Stoping Method at Trepça Underground Mine", Ph.D. Dissertation. Eskişehir Osmangazi University, Eskişehir.

Idris, M.A., Saiang, D. and Nordlund, E. (2015), "Stochastic assessment of pillar stability at Laisvall mine using artificial neural network", *Tunn. Undergr. Sp. Technol*., **49**, 307-319. https://doi.org/10.1016/j.tust.2015.05.003.

Itasca. (2005), FLAC3D-Fast lagrangian analysis of continua-user manual, ver. 2.21, Itasca Consulting Group, Minneapolis.

Jawed, M. and Sinha, R.K. (2018), "Design of rhombus coal pillars and support for roadway stability and mechanizing loading of face coal using SDLs in a steeply inclined thin coal seam-a technical feasibility study", *Arab. J. Geosci*., **11**, 415. https://doi.org/10.1007/s12517-018-3747-4

Jessu, K., Spearing, A. and Sharifzadeh, M. (2018), "Laboratory and numerical investigation on strength performance of inclined pillars", *Energies*, **11**(11), 3229. https://doi.org/10.3390/en11113229.

Kaiser, P.K., Kim, B., Bewick, R.P. and Valley, B. (2010), "Rock mass strength at depth and implications for pillar design", *Proceedings of the 5th international seminar on deep and high stress mining*. Santiago, Chile.

Khawar, M. (2013), "Development of correlation between rock classification system and modulus of Deformation", University of Engineering and Technology, Lahore.

Krauland, N. and Soder, P.E. (1987), "Determining pillar strength from pillar failure observation", *Eng. Min. J*., **8**, 34-40.

Kumar, H., Deb, D. and Chakravarty, D. (2017), "Numerical analysis of sill and crown pillar stability for multilevel cut and fill stopes in different geomining conditions", *Geotech. Geol. Eng*., **34**, 529-549. https://doi.org/10.1007/s10706-015-9964-7.

Lang, B.D.A. (1994), "Span Design for Entry-Type Excavations", Ph.D. Dissertation. University of British Columbia, Vancouver.

Li, X., Li, D., Liu, Zh., Zhao, G. and Wang, W. (2013), "Determination of the minimum thickness of crown pillar for safe exploitation of a subsea gold mine based on numerical

modeling", *Int. J. Roc. Mech. Min. Sci*., **57**(3), 42-56. https://doi.org/10.1016/j.ijrmms.2012.08.005.

Lunder, P. (1994), "Hard rock pillar strength estimation: an applied empirical approach", MSc Thesis. University of British Columbia, Vancouver.

Lunder, P.J. and Pakalnis, R.C. (1997), "Determination of the strength of hard-rock mine pillars", *Bull. Can. Inst. Min. Metall*., **90**, 51-55.

Marinos, P. and Hoek, E. (2000), "GSI: a geologically friendly tool for rock mass strength estimation", *Proceedings of the GeoEng2000 at the Int Conf on Geotechnical and Geological Engineering*.

Mark, C. and Bieniawski, Z.T. (1986), "An empirical method for the design of chain pillars in longwall mining", *Proceedings of the 27th U.S. Symposium on Rock Mechanics*, New York.

Martin, C.D. and Maybee, W.G. (2000), "The strength of hard-rock pillars", *Int. J. Roc. Mech. Min. Sci*., **37**, 1239-1246.

Mitri, H.S. (2007), "Assessment of horizontal pillar burst in deep hard rock mines", *Int. J. Risk Ass. Manag*., **7**(5), 695-707. https://doi.org/10.1504/IJRAM.2007.014094.

Mortazavi, A., Hassani, F.P. and Shabani, M. (2009), "A numerical investigation of rock pillar failure mechanism in underground openings", *Comp. Geo*., **36**, 691-697. https://doi.org/10.1016/j.compgeo.2008.11.004.

Naung, N., Sasaoka, T., Shimada, H. and Hamanaka, A. (2018), "Stability assessment of open stope under overlaying mined-out regions at Modi Taung gold mine, Myanmar", *Int. J. Geosc*., **9**(9), 547-571. https://doi.org/10.4236/ijg.2018.99032.

Nicholson, G.A. and Bieniawski, Z.T. (1990), "A nonlinear deformation modulus based on rock mass classification", *Int. J. Min. Geol. Eng*., **8**, 181-202.

Oke, J. and Kalenchuk, K. (2017), "Selecting the most applicable hard rock pillar design method", *Proceedings of the 51st US Rock Mechanics/Geomechanics Symposium*, California, USA.

Ouchi, A.M., Pakalnis, R. and Brady, T.M. (2004), "Update of span design curve for weak rock masses", *Proceedings of the 99th Annual AGM-CIM Conference*, Edmonton.

Ozbay, M.U., Ryder, J.A. and Jager, A.J. (1995), "The design of pillar system as practiced in shallow hard-rock tabular mines in South Africa", *J. S. Afr. Inst. Min. Metall*., **95**, 7-18.

Palinkas, S.S., Palinkas, L.A., Renac, C.H., Spnagenberg, J.E., Lueders, V., Molnar, F. and Maliqi, G. (2013), "Metallogenic model of the Trepça Pb-Zn-Ag skarn deposit, Kosovo: evidence from fluid inclusions, rare earch elements, and stable isotope data", *Economic Geology*., **108**(1), 153-162. https://doi.org/10.2113/econgeo.108.1.135.

Pariseau, W.G., Duan, F. and Schmuck, S.H. (1984), "Numerical assessment of the influence of anisotropy on steeply dipping VCR stopes", *SME-AMI*, New York.

Paveley, L.A. and Harding, R.B. (2011), "Pillar Optimization? Post-Pillar Cut and Fill Mining in a shallow dipping Ni Sulfide deposit in Northern Manitoba", *Can. Inst. Min. Metall. Pet*.

Potvin, Y., Hudyma, M. and Miller, H.D.S. (1989), "Rib pillar design in open stope mining", *Bull. Can. Inst. Min. Metall*., **82**(927), 31-36.

Ramamurthy, T. (2004), "A geo-engineering classification for rocks and rock masses", *Int. J. Roc. Mech. Min. Sci*., **41**, 89-101. https://doi.org/10.1016/S1365-1609(03)00078-9.

Read, S.A.L., Richards, L.R. and Perrin, N.D. (1999), "Applicability of the Hoek-Brown failure criterion to New Zealand greywacke rocks", *Proceedings of the 9th international symposium on rock mechanics*, Paris.

Ren, Q., Wang, F., Chen, B., Zhao, M., Peng, Z. and Yang, M. (2020), "Stability prediction of pillars based on Bieniawski pillar strength formula: a case of a phosphate mine", *Geotech. Geol. Eng*., **38**, 4033-4044. https://doi.org/10.1007/s10706-020-01275-9.

Sainoki, A. and Mitri, H.S. (2017), "Numerical investigation into pillar failure induced by time-dependent skin degradation", *Int. J. Min. Sci. Technol*., **27**(4), 591-7. https://doi.org/10.1016/j.ijmst.2017.05.002.

Salamon, M.D.G. and Munro, A.H. (1967), "A study of the strength of coal pillars", *J. S. Afr. Inst. Min. Metall*., **68**, 55-67.

Schubert, C.J. and Villaescusa, E. (2008), "An approach to hard rock pillar design at the McArthur River Mine", *Proceedings of the AusIMM Annual Conference*, Mount Isa.

Serafim, J.L. and Pereira, J.P. (1983), "Considerations of geomechanics classification of Bieniawski", *Proceedings of the International Symposium on engineering geology and underground construction*, Rotterdam, Balkema.

Sharipov, A.S. and Adoko, A.C. (2021), "An approach to estimate coal pillar strength", *Proceedings of the IOP Conference Series: Earth and Environmental Science.*, **833**(1), 012136. https://doi.org/10.1088/1755-1315/833/1/012136.

Sherizadeh, T. and Kulatilake, P.H.S.W. (2016), "Assessment of roof stability in a room and pillar coal mine in the U.S. using three-dimensional distinct element method", *Tunn. Undergr. Sp. Technol.*, **10**, 24-37. https://doi.org/10.1016/j.tust.2016.06.005.

Sjöberg, J. (1993), "Design methods for stope and sill pillars with application to the Zinkgruvan Mine", *Roc. Mech. Roc. Eng*., **26**(3), 253-275.

Sönmez, H., Gökçeoğlu, C. and Ulusay, R. (2004), "Indirect determination of the modulus of deformation of rock masses based on the GSI system", *Int. J. Roc. Mech. Min. Sci*., **41**(5), 849-857. https://doi.org/10.1016/j.ijrmms.2003.01.006.

Thibodeau, D. and Yao, M. (2015), "Post-pillar design for overhand cut and fill mining in moderate to high stress conditions: A case study", *Proceedings of the 13th ISRM International Congress of Rock Mechanics,* Montreal.

Ünlü, T. (2000), "Critical dimension concept in pillar stability", *Proceedings of the 17th International Mining Congress and Exhibition of Turkey*: *IMCET*, Ankara, Turkey.

Van der Merwe, J. and Mathey, M. (2013), "Update of coal pillar Database for South African coal mining", *J. S. Afr. Ins. Min. Metal.*, 113, 825-40. https://doi.org/10.1088/1755-1315/833/1/012136.

Vasarhelyi, B. and Kovacs, D. (2017), "Empirical methods of calculating the mechanical parameters of the rock mass", *Periodica Polytechnica Civil Eng.*, **61**(1), 38-50. https://doi.org/10.3311/PPci.10095.

Von Kimmelmann, M.R., Hyde, B. and Madgwick, R.J. (1984), "The use of computer applications at BCL Limited in planning pillar extraction and the design of mining layouts", *ISRM/BGS*, Cambridge.

Wagner, H. (2003), "The role of pillars in small underground mines", *International Conference on Safety and* Environment *Aspects of Mining*., **63**, 89-104.

Wang, J., Milne, D. and Pakalnis, R. (2002), "Application of a neural network in the empirical design of underground excavation spans", *Min. Technol*., **111**(1), 73-81. https://doi.org/10.1179/mnt.2002.111.1.73.

Wang, J., Pakalnis, R.., Milne, D. and Lang, B. (2000), "Empirical underground entry-type excavation span design modification", *Proceedings of the 53rd Annual Conference of the Canadian Geotechnical Society*, Montreal.

Zeqiri, K. (2020), "Investigation of the mining accidents at Stan Terg mine", *Min. Sci*., **27**, 39-46. https://doi.org/10.37190/msc202703.

Zhang, J., Peng, H., Qiang, Z., Meng, L. and Zhi-wei, C. (2017), "Stability and control of room mining coal pillars-taking room mining coal pillars of solid backfill recovery as an example", *J. Cen. S. Uni*., **24**(5), 1121-1132. https://doi.org/10.1007/s11771-017-3515-8

Zhou, N., Yan, H., Jiang, Sh., Sun, Q. and Ouyand, S. (2019), "Stability analysis of surrounding rock in paste backfill recovery of residual room pillars", *Susta. O. Ac, J*., **11**:1-13. https://doi.org/10.3390/su11020478.

CC